NASA TECHNICAL NOTE

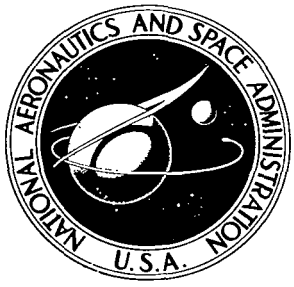

A METHOD FOR SOLVING THE NONSIMILAR LAMINAR BOUNDARY-LAYER EQUATIONS INCLUDING FOREIGN GAS INJECTION

by Joseph G. Marvin and Yvonne S. Sheaffer

Ames Research Center

Moffett Field, Calif.

NATIONAL AERONAUTICS AND SPACE ADMINISTRATION • WASHINGTON, D. C. • NOVEMBER 1969

1. Report No. NASA TN D-5516	2. Government Accession No.	3. Recipient's Catalog No.
4. Title and Subtitle A METHOD FOR SOLVING THE NONSIMILAR LAMINAR BOUNDARY-LAYER EQUATIONS INCLUDING FOREIGN GAS INJECTION		5. Report Date November 1969 6. Performing Organization Code
7. Author(s) Joseph G. Marvin and Yvonne S. Sheaffer		8. Performing Organization Report No. A-3354
9. Performing Organization Name and Address NASA Ames Research Center Moffett Field, Calif. 94035		10. Work Unit No. 129-01-03-07-00-21 11. Contract or Grant No.
12. Sponsoring Agency Name and Address National Aeronautics and Space Administration Washington D. C. 20546		13. Type of Report and Period Covered TECHNICAL NOTE 14. Sponsoring Agency Code

15. Supplementary Notes

16. Abstract

A numerical method for solving the nonsimilar boundary-layer equations, including binary gas injection, is developed for nonreacting gases. The continuity, momentum, energy, and species-concentration equations and boundary conditions are reduced to a set of linear algebraic equations in terms of the dependent variables only by appropriate application of implicit finite difference expressions. To solve the equations, profiles of the unknowns at the initial station are specified, together with certain boundary conditions along the body surface and boundary-layer edge. The initial profiles are obtained through solution, by the same method, employing the similarity form of the conservation equations that apply exactly at the starting points for the problems considered.

Comparisons of the present solutions with exact similarity solutions for air and helium injection are presented to demonstrate the accuracy of the method for evaluating the dependent variables along the initial data line. Comparisons of the present solutions with nonsimilar solutions obtained from other numerical methods and comparisons with experimental data for air, argon, and helium injection are presented to evaluate the accuracy and advantages of the method.

17. Key Words Suggested by Authors	18. Distribution Statement
Boundary Layer Foreign Gas Injection Finite Differences	UNCLASSIFIED - UNLIMITED

19. Security Classif. (of this report)	20. Security Classif. (of this page)	21. No. of Pages	22. Price*
UNCLASSIFIED	UNCLASSIFIED	29	$3.00

*For sale by the Clearinghouse for Federal Scientific and Technical Information
Springfield, Virginia 22151

A METHOD FOR SOLVING THE NONSIMILAR LAMINAR BOUNDARY-LAYER EQUATIONS INCLUDING FOREIGN GAS INJECTION

By Joseph G. Marvin and Yvonne S. Sheaffer

Ames Research Center

SUMMARY

A numerical method for solving the nonsimilar boundary-layer equations, including binary gas injection, is developed for nonreacting gases. The continuity, momentum, energy, and species-concentration equations and boundary conditions are reduced to a set of linear algebraic equations in terms of the dependent variables only by appropriate application of implicit finite difference expressions. To solve the equations, profiles of the unknowns at the initial station are specified, together with certain boundary conditions along the body surface and boundary-layer edge. The initial profiles are obtained through solution, by the same method, employing the similarity form of the conservation equations that apply exactly at the starting points for the problems considered.

Comparisons of the present solutions with exact similarity solutions for air and helium injection are presented to demonstrate the accuracy of the method for evaluating the dependent variables along the initial data line. Comparisons of the present solutions with nonsimilar solutions obtained from other numerical methods and comparisons with experimental data for air, argon, and helium injection are presented to evaluate the accuracy and advantages of the method.

INTRODUCTION

At the inception of this investigation, wind-tunnel tests were planned that involved foreign gas injection through a porous model. To meet the requirements for data correlations, it was necessary to calculate various boundary-layer parameters that required solutions to the nonsimilar boundary-layer equations including foreign gas injection. A computer program utilizing the Smith-Clutter approach was available for solving the nonsimilar equations (see, e.g., refs. 1 and 2). While experience has shown this program was useful for studying the effects of pressure gradient without injection (see refs. 3 and 4), computer time and convergence limitations made it impractical for the present application. Therefore, a finite difference method for solving the nonsimilar equations including binary gas injection was developed to circumvent these limitations.

Finite difference schemes can be categorized as explicit or implicit. The explicit schemes are conditionally stable; for most applications, the Δx step size becomes impractically small and resulting computing times excessively long (see ref. 5). The implicit schemes, on the other hand, are usually unconditionally stable. Flügge-Lotz and Blottner (ref. 6) took advantage of this fact to demonstrate the utility and speed of an implicit scheme for solving the boundary-layer equations. Blottner later applied this technique (ref. 7) to solve the complicated nonequilibrium boundary-layer problem. Although the method described in reference 6 has many advantages, it was not applied extensively until recently (e.g., refs. 8 and 9).

The present work uses the basic implicit scheme described in reference 6, but here the basic equations are transformed to new coordinates with finite boundaries by means of a transformation described in reference 10. The asymptotic nature of the transformation allows the choice of a constant $\Delta\bar{y}$ step size within finite limits (say, between 0 and 1), thus eliminating the necessity of searching for the effective boundary-layer edge through additional iteration. Subsequent to the coordinate transformation, the equations are put in finite difference form so that the unknowns appear linearly. The resulting set of linear algebraic equations and a stream-function equation are solved on a digital computer after specifying streamwise boundary conditions along the body surface and boundary-layer edge and profiles of the unknowns at the initial streamwise location. The initial profiles are obtained by the same method employing the similarity form of the equations that apply exactly at the streamwise starting locations for the problems considered.

This report presents the solution method and demonstrates, by example, its capabilities and accuracy. Although the original application of the method was specifically directed toward solutions that included binary injection, the method is applicable to many other boundary-layer problems.

SYMBOLS

A_n, B_n, C_n coefficient matrices given in equation (23)

C mass concentration

C_p frozen specific heat at constant pressure, see equation (18)

C_v specific heat at constant volume

$\bar{\bar{D}}_n$ solution vector (column matrix) in equation (23)

D^* total displacement thickness with mass addition, see equation (39)

D_{12} binary diffusion coefficient

E	defined by equations (28) and (29)
F	defined by equation (4)
f	stream function, $\int^{\eta} \frac{u}{u_e} d\eta$
G	dummy variable
$\bar{\bar{g}}$	edge boundary-condition vector
H	boundary-condition coefficient matrix
$\bar{\bar{h}}$	wall boundary-condition vector denoting column matrix
$\bar{\bar{J}}$	vector denoting column matrix given by equation (28)
K	weighting factor in transport coefficients, see equation (22)
k	thermal conductivity
L	length of nonporous tip
M	dummy variable
M	molecular weight
m	mesh point in x direction
N	denotes number of mesh points in y direction
n	mesh point in y direction, n = 1,2, . . . , N
P	coefficient in polynomial expressions for properties, see equation (15)
p	pressure
Pr	Prandtl number, $C_p \frac{\mu}{k}$
q	heat-transfer rate
R	dummy variable
$\mathfrak{R}$	universal gas constant
r	normal distance from axis of symmetry to body surface
S	dimensionless distance along surface in flow direction $\frac{\xi}{\xi_l}$
Sc	Schmidt number, $\frac{\mu}{\rho D_{12}}$

T	normalized temperature, $\frac{t}{t_o}$
t	temperature
u	velocity in streamwise direction
v	velocity normal to streamwise direction
X	mole fraction
$\bar{x}$	streamwise distance from tip of body
$\bar{y}$	normal distance from body surface
y	transformed normal distance defined by equation (7)
Z	stretched normal distance, $\alpha(1 - y)$
α	scale factor in equation (7)
β	pressure gradient parameter, $\frac{2\xi}{u_e}\frac{du_e}{d\xi}$
δ^*	displacement thickness given by equation (38)
ϵ	wall boundary conditions on species (eqs. (26) and (30))
η	transformed normal coordinate (eq. (5))
θ	momentum thickness given by equation (40)
μ	viscosity
ξ	transformed streamwise coordinate (eq. (6))
ρ	density
$\vec{\omega}$	vector denoting column matrix for unknowns at (m + 1), see equation (23)
τ	shear stress defined by equation (33)
ϕ	dimensionless density-viscosity product, $\frac{\rho\mu}{\rho_e\mu_e}$
Δy	step size in y direction

Subscripts

a,b,c,d,e,f	mesh points for finite difference scheme (see sketch (b))
e	boundary-layer-edge value
i	species i; i = 1 is free stream, i = 2 is injectant
I	initial value
k	coefficient number in polynomial for thermodynamic and transport properties
ℓ	evaluated at arbitrary length, $\bar{x} = \ell$
o	stagnation-point value
NS	nonsimilar value
S	similar value
y,η,s,ξ	partial differentiation with respect to the subscript
W	wall value
1	free-stream species
2	injected species

Superscripts

ν	iteration number
n	geometric factor; n = 0 is two-dimensional and n = 1 is axisymmetric
k	polynomial degree

ANALYSIS

The nonsimilar, laminar boundary-layer equations are given in this section, along with the equations for evaluating the thermodynamic and transport properties of the binary gas systems considered. The method of solution, involving a transformation and a linearization of the boundary-layer equations, is presented and equations are given for determining shear stress, heat transfer, and other important boundary-layer parameters.

Boundary-Layer Equations

The mass, momentum, energy, and species conservation equations for a binary gas system in the familiar Levy-Lees variables (e.g., ref. 2) are:

Momentum

$$(\phi F_\eta)_\eta + fF_\eta + \beta(\rho_e/\rho - F^2) = 2\xi(FF_\xi - F_\eta f_\xi) \tag{1}$$

Energy

$$\frac{1}{C_p}\left(\frac{\phi}{Pr} C_p T_\eta\right)_\eta + fT_\eta + \frac{\phi}{ScC_p}\left(C_{p_1} - C_{p_2}\right)C_{1_\eta} T_\eta + \frac{\phi u_e^2}{C_p t_o} F_\eta^2 - \frac{\beta u_e^2}{C_p t_o}\frac{\rho_e}{\rho} F$$

$$= 2\xi\left(FT_\xi - T_\eta f_\xi\right) \tag{2}$$

Species (binary system)

$$\left(\frac{\phi}{Sc} C_{1_\eta}\right)_\eta + fC_{1_\eta} = 2\xi\left(FC_{1_\xi} - C_{1_\eta} f_\xi\right) \tag{3}$$

where

$$F = f_\eta = \frac{u}{u_e} \tag{4}$$

$$\eta = \frac{r^n \rho_e u_e}{\sqrt{2\xi}} \int_0^{\bar{y}} \frac{\rho}{\rho_e}\, d\bar{y} \tag{5}$$

$$\xi = \int_0^x \rho_e u_e \mu_e r^{2n}\, d\bar{x} \tag{6}$$

The boundary conditions are

$\eta = 0$

$$F = 0$$

$$T = T_w$$

$$\left(C_1\right)_\eta = \frac{\sqrt{2\xi}\left(C_1\right)_w (\rho v)_w Sc_w}{\rho_w \mu_w u_e r^n}$$

$$f(0) = -\frac{1}{\sqrt{2\xi}} \int_{\bar{x}_I}^{\bar{x}} (\rho v)_w r^n\, d\bar{x}$$

$\eta \to \infty$

$$F \to 1$$

$$T \to T_e$$

$$C_1 \to 1$$

The boundary conditions at $\eta = 0$ are based on the assumption that the net mass flow of the free-stream gas at the wall is zero (e.g., ref. 2).

Transformation to Finite Coordinates

It is convenient from a computational viewpoint to transform the above equations to a new system of coordinates wherein the indefinite limit of integration on η is replaced by a definite limit (e.g., ref. 10). Let

$$y = 1 - e^{-\alpha\eta} \tag{7}$$

For a system of finite-difference equations with a fixed number of y nodal points and a fixed interval Δy, α is used as a scaling factor to provide an optimum distribution of nodal points across the boundary layer. A certain amount of experience is required to achieve the optimum results, as will be discussed subsequently.

The following transformation identities result

$$\begin{aligned} (\ )_\eta &= \alpha(1 - y)(\ )_y \\ (\ )_{\eta\eta} &= \alpha^2(1 - y)[(1 - y)(\ )_{yy} - (\ )_y] \end{aligned} \tag{8}$$

Employing these transformation identities, equations (1) through (4) become

Momentum

$$\alpha^2(1 - y)^2\phi_y F_y + \phi\alpha^2(1 - y)^2F_{yy} - \phi\alpha^2(1 - y)F_y + \alpha(1 - y)fF_y + \beta(\rho_e/\rho - F^2) = 2\xi[FF_\xi - \alpha(1 - y)F_y f_\xi] \tag{9}$$

Energy

$$\frac{1}{C_p}\alpha^2(1- y)^2\left(\frac{\phi C_p}{Pr}\right)_y T_y + \frac{\phi}{Pr}\alpha^2(1 - y)[(1 - y)T_{yy} - T_y] + \alpha f(1 - y)T_y + \frac{\phi}{ScC_p}\left(C_{p_1} - C_{p_2}\right)\alpha^2(1 - y)^2C_{1_y}T_y - \frac{\beta u_e^2}{C_p t_o}\frac{\rho_e}{\rho}F + \frac{\phi u_e^2}{C_p t_o}\alpha^2(1 - y)^2F_y^2 = 2\xi[FT_\xi - \alpha(1 - y)T_y f_\xi] \tag{10}$$

Species

$$\alpha^2(1 - y)^2 C_{l_y}\left(\frac{\phi}{Sc}\right)_y + \frac{\phi}{Sc}\alpha^2(1 - y)^2 C_{l_{yy}} - \frac{\phi}{Sc}\alpha^2(1 - y)C_{l_y} + \alpha f(1 - y)C_{l_y}$$

$$= 2\xi\left[FC_{l_\xi} - \alpha(1 - y)C_{l_y}f_\xi\right] \qquad (11)$$

where

$$f = \int_0^y \frac{F}{\alpha(1 - y)}\,dy + f(0) \qquad (12)$$

The boundary conditions become for $y = 0$

$$\left.\begin{aligned} F &= 0 \\ T &= T_w \\ \left(C_l\right)_y &= \frac{\sqrt{2\xi}\,C_{l_w}(\rho v)_w Sc_w}{\alpha\rho_w\mu_w u_e r^n} \\ f(0) &= -\frac{1}{\sqrt{2\xi}}\int^x (\rho v)_w r^n\,d\bar{x} \end{aligned}\right\} \qquad (13)$$

and for $y = 1$

$$\left.\begin{aligned} F &= 1 \\ T &= T_e \\ C_l &= 1 \end{aligned}\right\} \qquad (14)$$

Thermodynamic and Transport Properties

To complete the system of equations, the thermodynamic and transport properties are expressed as functions of the dependent variables C_l and T in the manner described in reference 2. The properties of the individual gas constituents were expressed as polynomials in terms of temperature; for example,

$$C_{p_i} = \sum_0^k P_k T^k \qquad (15)$$

A similar expression was used for μ_i and D_{12}. Values of the coefficients, P_k,

used to obtain C_{p_i}, μ_i, and D_{ij} for the gases considered are given in reference 2, along with a brief description of the assumptions regarding intermolecular potentials.

The thermal conductivity of each constituent was obtained from Eucken's relation

$$k_i = \frac{1}{4}\left(9\,\frac{C_{p_i}}{C_{v_i}} - 5\right)C_{v_i}\mu_i \tag{16}$$

where

$$C_{v_i} = C_{p_i} - \frac{\Re}{M_i} \tag{17}$$

Mixture values of the thermodynamic and transport properties were obtained from the equations:

$$C_p = C_{p_2} + C_1\left(C_{p_1} - C_{p_2}\right) \tag{18}$$

$$\rho = \frac{p}{\Re T}\left[\frac{M_1 M_2}{M_1 + C_1(M_2 - M_1)}\right] \tag{19}$$

Mixture values of the transport properties were obtained from the approximate combining equations taken from reference 11:

$$k = \frac{k_1}{1 + 1.065K_{12}\,\frac{X_2}{X_1}} + \frac{k_2}{1 + 1.065K_{21}\,\frac{X_1}{X_2}} \tag{20}$$

$$\mu = \frac{\mu_1}{1 + K_{12}\,\frac{X_2}{X_1}} + \frac{\mu_2}{1 + K_{21}\,\frac{X_1}{X_2}} \tag{21}$$

where

$$K_{12} = \frac{\left[1 + (\mu_1/\mu_2)^{1/2}(M_2/M_1)^{1/4}\right]^2}{2^{3/2}\left(1 + M_1/M_2\right)^{1/2}} \tag{22}$$

and where K_{21} is obtained from equation (22) with subscripts 1 and 2 interchanged.

Method of Solution

To obtain a numerical solution, equations (9) through (11) are approximated by a set of implicit finite difference equations of the Crank-Nicholson type and the ensuing tridiagonal matrix equations $A\bar{\bar{\omega}} = \bar{\bar{D}}$, solved on a computer by the algorithm given in reference 12. To use the solution algorithm, the equations must be linearized, values for the unknowns at the initial streamwise location must be specified along with streamwise boundary conditions at the wall and the boundary-layer edge. In the subsequent portions of this section, the difference equations, the boundary conditions, and the solution are discussed.

The mesh-point diagram for the Crank-Nicholson scheme is shown below. The finite-difference equations used to assure linear equations when marching from line (m) to (m + 1) are given in appendix A.

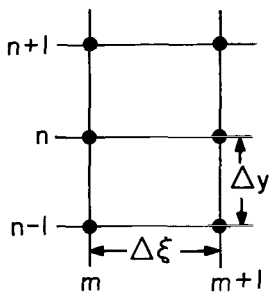

Sketch (a)

Substituting the difference equations into the momentum, energy, and species equations (eqs. (9) - (11)) results in 3(N - 2) linear equations. In matrix equation form, one obtains

$$A_n\bar{\bar{\omega}}_{n-1} + B_n\bar{\bar{\omega}}_n + C_n\bar{\bar{\omega}}_{n+1} = \bar{\bar{D}}_n \qquad n = 2,3, \ldots ,N-1 \tag{23}$$

where, for example, the vectors and coefficient matrices have the following form

$$\bar{\bar{\omega}}_n = \begin{bmatrix} F \\ T \\ C_1 \end{bmatrix}_{n,m+1} \qquad \bar{\bar{D}}_n = \begin{bmatrix} D_1 \\ D_2 \\ D_3 \end{bmatrix}_{\substack{n,m \\ \text{or } n,m+1/2}} \qquad A_n = \begin{bmatrix} A_{11} & 0 & 0 \\ A_{21} & A_{22} & A_{23} \\ 0 & 0 & A_{33} \end{bmatrix}_{\substack{n,m \\ \text{or } n,m+1/2}}$$

As shown in appendix A, the matrices B_n and C_n are similar in form to A_n, except $B_{23} = 0$. The matrices A_n, B_n, and C_n, and the solution vector $\bar{\bar{D}}_n$, are considered known and are evaluated at (n, m) or (n, m + 1/2) depending on the iteration described subsequently. Equations for the matrix elements and vector $\bar{\bar{D}}_n$ are given in appendix A.

To complete the system of equations, values of the dependent variables $\bar{\bar{\omega}}_n$ at the two boundaries must be specified. To be consistent with the solution algorithm in reference 12, these were written as

$$\left.\begin{aligned} y = 0 \qquad \bar{\bar{\omega}}_1 &= H\bar{\bar{\omega}}_2 + \bar{\bar{h}} \\ y = 1 \qquad \omega_N &= \bar{\bar{g}} \end{aligned}\right\} \tag{24}$$

Special attention was given to the boundary condition on wall concentration to arrive at a form consistent with equation (24). The condition was obtained by expressing the concentration at $n = 2$ in finite difference form as a Taylor series about $n = 1$ and retaining three terms.

$$(C_1)_2 = C_1(\Delta y) = C_1(0) + \Delta y\,[C_1(0)]_y + \frac{\Delta y^2}{2}[C_1(0)]_{yy} \tag{25}$$

The terms $[C_1(0)]_y$ and $[C_1(0)]_{yy}$ are obtained from the boundary condition, equation (13), and equation (11) evaluated at $y = 0$. After some manipulation, equation (25) is rewritten as

$$C_1(0) = \frac{C_1(\Delta y)}{1 + \varepsilon_{NS}} \tag{26}$$

where

$$\varepsilon_{NS} = \frac{\sqrt{2\xi}\,Sc_w(\rho v)_w}{\alpha(\rho\mu)_w u_e r^n}\left[\Delta y + \frac{\Delta y^2}{2}\left(1 - \frac{Sc_w}{\phi_w}\left(\frac{\phi_w}{Sc_w}\right)_y + \frac{\sqrt{2\xi}\,(\rho v)_w Sc_w}{\alpha(\rho\mu)_w u_e r^n}\right)\right]$$

Using equation (26) together with equations (13) and (14), the elements of the matrix coefficient and vectors in equations (24) become

$$H = \begin{bmatrix} 0 & 0 & 0 \\ 0 & 0 & 0 \\ 0 & 0 & \dfrac{-1}{1 + \varepsilon_{NS}} \end{bmatrix}_{n,m \text{ or } n,m+1/2} \qquad \bar{\bar{h}} = \begin{bmatrix} 0 \\ T_W \\ 0 \end{bmatrix}_{n,m+1} \qquad \bar{\bar{g}} = \begin{bmatrix} 1 \\ T_e \\ 1 \end{bmatrix}_{n,m+1}$$

Equations (23), together with the boundary conditions, equations (24), form a set of linear equations which can be solved on a digital computer once profiles of the dependent variables at an initial streamwise location are specified. The algorithm for solution, taken from reference 12, is

$$\bar{\bar{\omega}}_n = -E_n\bar{\bar{\omega}}_{n+1} + \bar{\bar{J}}_n \qquad 1 \le n \le N - 1 \tag{27}$$

where

$$E_n = (B_n - A_nE_{n-1})^{-1}C_n$$

$$\bar{\bar{J}}_n = (B_n - A_nE_{n-1})^{-1}(\bar{\bar{D}}_n - A_n\bar{\bar{J}}_{n-1}) \qquad 2 \le n \le N - 1 \tag{28}$$

and where

$$\begin{aligned} E_1 &= H & E_N &= 0 \\ \bar{\bar{J}}_1 &= \bar{\bar{h}} & \bar{\bar{J}}_N &= \bar{\bar{g}} \end{aligned} \tag{29}$$

The computation proceeds with evaluation of equations (28) from the wall to the boundary-layer edge using matrix elements based on values of the dependent variables and appropriate derivatives evaluated at m. Values of the dependent variable $\bar{\bar{\omega}}_n$ at (m + 1) are determined in reverse order using equations (27) and (29). New values of the stream function f are obtained by integrating equation (12). Values of the streamwise derivatives of f are redetermined and the new values for f and $\bar{\bar{\omega}}_n$ are averaged over the interval with corresponding values at m to form new matrix elements at (n, m + 1/2). The solution was iterated until

$$\frac{\left|[F(0)]_y^{\nu+1} - [F(0)]_y^{\nu}\right|}{[F(0)]_y^{\nu+1}} \leq 0.0005$$

(For all computations made thus far, this criterion was sufficient to assure convergence of temperature and concentration profiles.)

To start the solutions, values of the dependent variables $\bar{\bar{\omega}}_n$ and the stream function f at the initial station ξ_I, must be specified. From an appropriate starting point these values can be obtained by solving the similarity form of the boundary-layer equations obtained by setting the right-hand sides of equations (9) through (11) to zero (i.e., visualize a stagnation point, or a point along the surface of a cone with uniform free-stream conditions and $f(0) = 0$ or $f(0) \sim 1/\sqrt{x}$). The similarity form of the equations were solved by a method analogous to that described above. The mesh-point diagram and finite difference approximations are given in appendix B. Substituting the difference equations from appendix B into equations (9) through (11) with the right-hand sides set to zero also results in 3(N - 2) linear equations of the form given by equation (23). The equations for the coefficient matrix elements and vector $\bar{\bar{D}}_n$ are given in appendix B. The boundary conditions and solution algorithm remain unchanged, except that the term ε_{NS} in the concentration boundary condition becomes

$$\varepsilon_S = \frac{\sqrt{2\xi}\ Sc_w(\rho v)_w}{\alpha(\rho\mu)_w u_e r^n}\left\{\Delta y + \frac{\Delta y^2}{2}\left[1 - \frac{Sc_w}{\phi_w}\left(\frac{\phi_w}{Sc_w}\right)_y - \frac{Sc_w}{\phi_w \alpha} f(0)\right]\right\} \tag{30}$$

and the boundary condition on the stream function becomes

$$f(0) = -\frac{(\rho v)_w \sqrt{2\xi}}{(\rho\mu)_e u_e r^n} \tag{31}$$

The similarity solution is started by assuming linear profiles of the dependent variables across the boundary layer to evaluate the matrix elements in equations (28). New values of the dependent variables are obtained from equations (27) and (29) and integration of equation (12). The new variables are then averaged with corresponding values of the variables from the previous iteration to form new matrix elements for equations (28). The solution was iterated until

$$\frac{\left|[F(0)]_y^{\nu+1} - [F(0)]_y^{\nu}\right|}{[F(0)]_y^{\nu+1}} \leq 0.0005$$

Boundary-Layer Parameters

In addition to using the solutions of the foregoing boundary-layer equations to obtain profiles of F, T, and C at each station along a body, other quantities can be computed as follows:

Skin friction.- The defining equation for wall skin friction is

$$\tau_w = \mu_w (u_{\bar{y}})_w \tag{32}$$

Transforming equation (32) to the present coordinate system gives

$$\tau_w = \frac{\alpha u_e^2 \rho_w \mu_w r^n}{\sqrt{2\xi}} (F_y)_w \tag{33}$$

The derivative $(F_y)_w$ was obtained by means of a three-point derivative equation and the converged solution for F

$$(F_y)_w = \frac{1}{2\ \Delta y}(-3F_w + 4F_{w+\Delta y} - F_{w+2\ \Delta y}) \tag{34}$$

Heat transfer.- The heat transfer to the wall was obtain from

$$q_w = -t_o k_w (T_{\bar{y}})_w = \frac{\alpha t_o \rho_w k_w r^n u_e}{\sqrt{2\xi}} (T_y)_w \tag{35}$$

where $(T_y)_w$ was obtained from the converged solution for T in an equation similar in form to equation (34). At a stagnation point, equation (35) reduces to

$$q_w = \alpha \rho_w k_w t_o \sqrt{2^n \frac{(du_e/dx)_o}{\rho_e u_e}} (T_y)_w \tag{36}$$

Displacement and momentum thicknesses.- Certain useful integrals of the profiles across the boundary layer can also be evaluated. The usual displacement thickness is given by

$$\delta^* = \int_0^{\bar{y}_e} \left(1 - \frac{\rho u}{\rho_e u_e}\right) d\bar{y} \tag{37}$$

In the present coordinate system this equation becomes

$$\delta^* = \frac{\sqrt{2\xi}}{\rho_e u_e r^n} \int_0^{y_e} \frac{(\rho_e/\rho) - F}{\alpha(1 - y)}\, dy \tag{38}$$

where y_e is the boundary-layer height at which $F = 0.995$. It should be noted that the thickness given by δ^* is not the displacement thickness required to describe physically the *free-stream* mass flow entrained in the boundary layer with injection. To obtain that thickness, as shown in reference 13, the appropriate expression is

$$D^* = \delta^* + \frac{1}{r^n} \int^{\bar{x}} \frac{(\rho v)_w}{\rho_e u_e} r^n \, d\bar{x} \tag{39}$$

The momentum thickness is given by the equation

$$\theta = \int_0^{\bar{y}_e} \frac{\rho u}{\rho_e u_e} \left(1 - \frac{u}{u_e}\right) d\bar{y} = \frac{\sqrt{2\xi}}{\rho_e u_e r^n} \int_0^{y_e} \frac{F(1 - F)}{\alpha(1 - y)} \, dy \tag{40}$$

RESULTS AND DISCUSSION

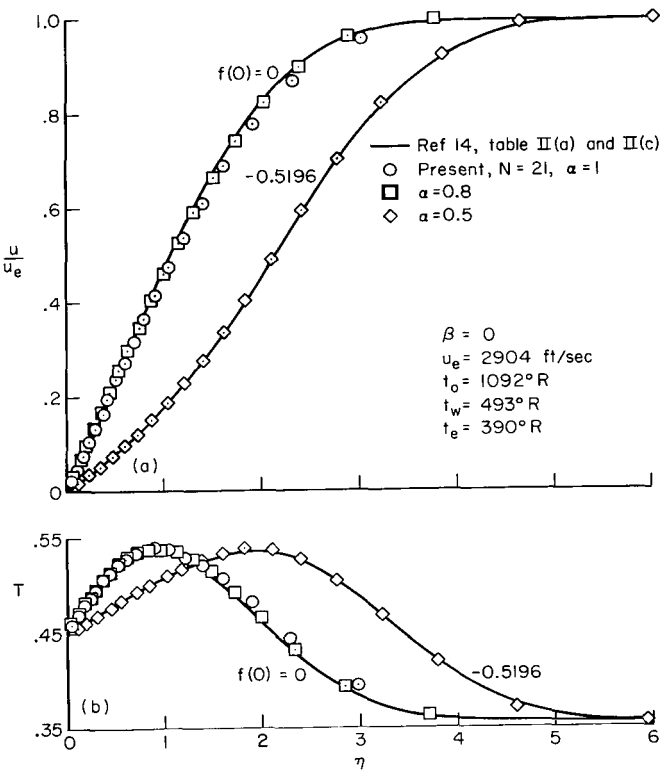

(a) Velocity profile.
(b) Temperature profile.

Figure 1.- Comparison of the present solution with the solution of Low, reference 14.

The foregoing equations were programmed in Fortran IV for solution on an IBM 7094 computer. The method of solution was verified by comparisons with numerical solutions obtained from other sources and by comparisons with experimental data. Some examples of these comparisons are given below to illustrate the capabilities and advantages of the method.

Similarity Solutions

As noted in the analysis section, a special finite-difference formulation was used to solve the similarity form of the boundary-layer equations. To verify this approach, a comparison with exact similarity solutions was made. Typical examples are discussed below.

Figure 1 shows a comparison with the velocity and temperature profiles from reference 14. Profiles, with and without air injection, are shown. (The linear

viscosity law reported in reference 14 was also employed in the present solutions to eliminate transport property differences.) Results from the present method were obtained for several values of the scale factor α using 21 nodal points (N) across the boundary layer. As mentioned previously, the choice of α determines the spacing of the nodal points across the layer and the choice has some influence on the solution in the outer portion of the boundary layer. See, for example, the solution for $f(0) = 0$ in figure 1. Experience has shown values of $\alpha \leq 0.5$ are required when injection is being considered. However, even for a poor choice of α, the profiles and derivatives of velocity and temperature near the wall are accurate enough for most practical applications. No attempt was made to determine the optimum combinations of α and N for this or any of the following examples.

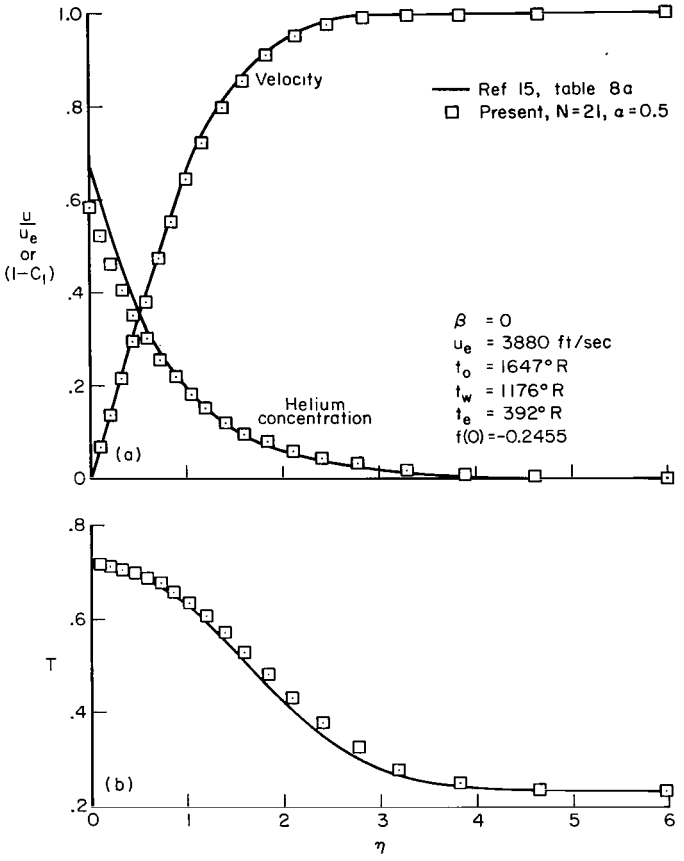

(a) Velocity and concentration.
(b) Temperature.

Figure 2.- Comparison of the present solution with the solution of Baron, reference 15.

A comparison of the present solution with the similarity solution from reference 15 for foreign gas injection is shown in figure 2. The thermodynamic and transport properties given in the analysis section were used for the present solutions, and these were not exactly the same as those reported in reference 15. Velocity, helium-concentration, and temperature profiles agree very well, except for differences in the concentration near the wall. The differences were attributed to the different transport properties employed in the two solutions.

Nonsimilar Solutions

The present method was verified primarily through comparisons with solutions using a modified form of the Smith-Clutter computer program (see refs. 1 and 3). In the Smith-Clutter method, the partial differential equations are reduced to ordinary differential equations in η by finite differencing derivatives in the ξ direction. The equations are solved by the so-called "shooting" technique - that is, as a two-point boundary-value problem prescribing initial conditions for derivatives of velocity and temperature at $\eta = 0$, and iteratively changing these conditions until the edge conditions are satisfied as $\eta \to \infty$.

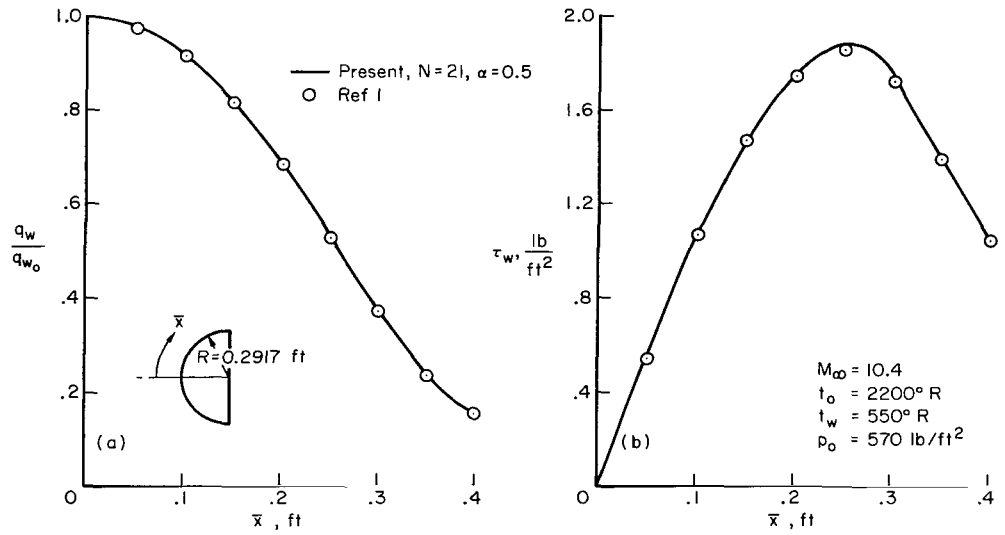

(a) Heating.
(b) Shear stress.

Figure 3.- Comparison of nonsimilar solutions for a sphere.

Figure 3 presents an example comparison of predicted heating rates and wall shear along the surface of a hemisphere. The same values of surface pressure and boundary-layer-edge velocity and temperature were used as input to both computer programs. Agreement between the two methods is excellent, as was the agreement between velocity and temperature profiles at various locations along the hemisphere. As described in the analysis section, initial profiles for the present method were obtained by solving the finite difference form of equations (9) through (12) at the stagnation point where $\xi = 0$. Computations were then made for the full set of equations at 92 locations along the hemisphere. The Δx step size was constant at a value of 0.005 ft. No attempt was made to determine the maximum Δx step size to achieve minimum computing time because such optimization would depend on body geometry and corresponding boundary-layer-edge conditions and the results would not be generally applicable to other examples. However, it is interesting to note that the present solutions required about 0.04 minute per body station versus about 0.7 minute per station for the method of reference 1.

A more stringent example is given in figure 4. Solutions were obtained for a cone with a sharp solid tip followed by a porous surface with uniform air injection (see ref. 16). The decrease in skin friction and accompanying increase in displacement thickness along the cone surface is compared with corresponding values obtained from the computer programs described in references 1 and 16. Boundary-layer-edge conditions and cone pressure were assumed constant in all programs. The starting profiles for the present solutions were obtained from the similarity form of equations (9) through (12), evaluated at $x = 0.158$ ft and for $f(0) = 0$. Solutions beyond this location were obtained from the complete equations with the prescribed value of $(\rho v)_w$. The Δx step size was 0.00025 ft for the first 21 computing stations and then was increased to 0.015 ft for the remaining stations. The small initial step size was chosen to avoid numerical instabilities due to the step change in $(\rho v)_w$.

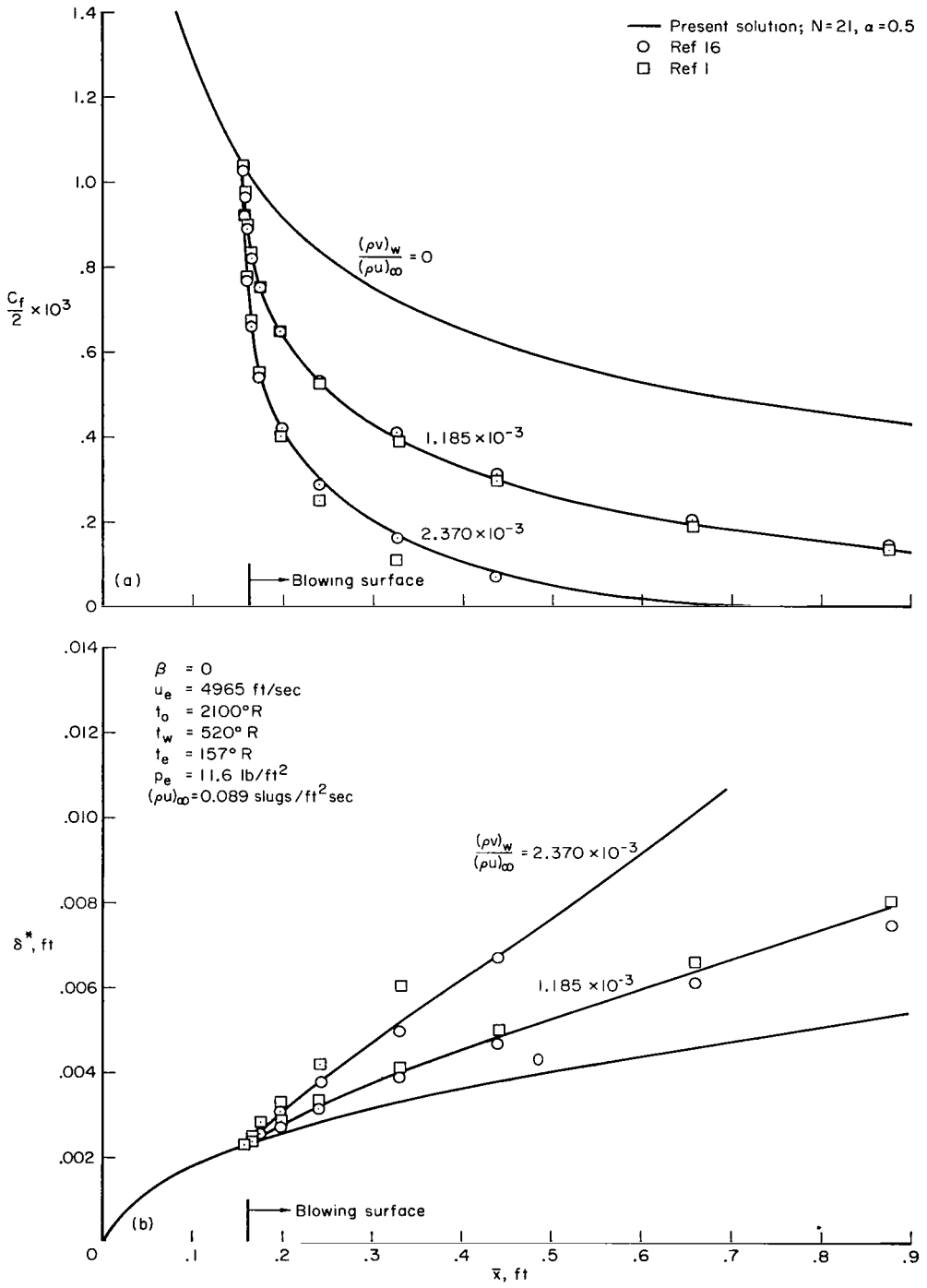

(a) Skin friction.
(b) Displacement thickness.

Figure 4.- Comparison of nonsimilar solutions for uniform air injection on a cone.

For the lowest injection rate, agreement with the other computed solutions is very good. For the highest injection rate considered $(\rho v)_w/(\rho u)_\infty = 2.37\times10^{-3}$, solutions using the "shooting" technique (ref. 1) did not satisfy the derivative boundary conditions as $\eta \to \infty$ for $x > 0.2$ ft; in addition, the program would not continue beyond $x = 0.325$ ft, whereas there was no difficulty in proceeding further with the present method and that of reference 16. The difficulty encountered by the "shooting" technique is typical of those encountered by this method when gradients of the dependent variables near the wall become small. The distinct advantage of the present method is that values of the dependent variables, rather than their slopes, are employed to obtain solutions. As a result, no difficulty has been encountered with injection problems where the skin friction or heat transfer become very small. This advantage would also be expected when solving problems with adverse pressure gradient approaching incipient separation. It is not known whether the method described in reference 16 also has these advantages. In the example above, the solution from reference 16 failed to converge at $x = 0.65$ ft (the next computing station), probably because the Δx step size was too large.

One of the purposes for developing the present finite-difference method of solution including foreign gas injection was to assist in data correlations of wind-tunnel experiments. A configuration currently under study is similar to that used in the previous example; that is, a 5° cone with a solid sharp tip followed by a uniformly porous conical surface. The predicted effects of gas injection for this test model are given below and compared with some experimental heat-transfer data taken at Ames Research Center in the 3.5-ft hypersonic wind tunnel (see ref. 17).

Figure 5 presents the predicted laminar boundary-layer heat transfer along the porous cone surface for three injectant gases and for several injectant rates. The predictions were obtained assuming uniform boundary-layer-edge conditions of Mach number, temperature, and pressure, and using the measured injection rate distribution from reference 17. The symbols represent measurements of the laminar boundary-layer heating rate obtained for each of the injectant rates. Only laminar boundary-layer heating data are shown in figure 5. Transition occurred and the heating rates increased downstream of the locations where these data are plotted. For each injectant gas, increasing the injectant rate decreased the heat transfer to a negligible value. For the same injectant rate the amount of heating reduction depended on the injectant gas molecular weight; compare, for example, the reductions for each injectant at $(\rho v)_w/\rho_\infty u_\infty = 1.1\times10^{-3}$. The agreement between theory and experiment is good, considering the experimental uncertainties in local injection rates and the fact that the theory did not account for the changes in boundary-layer-edge Mach number, temperature, and pressure resulting from displacement effects due to injection. The displacement effects are particularly important for the helium injection tests.

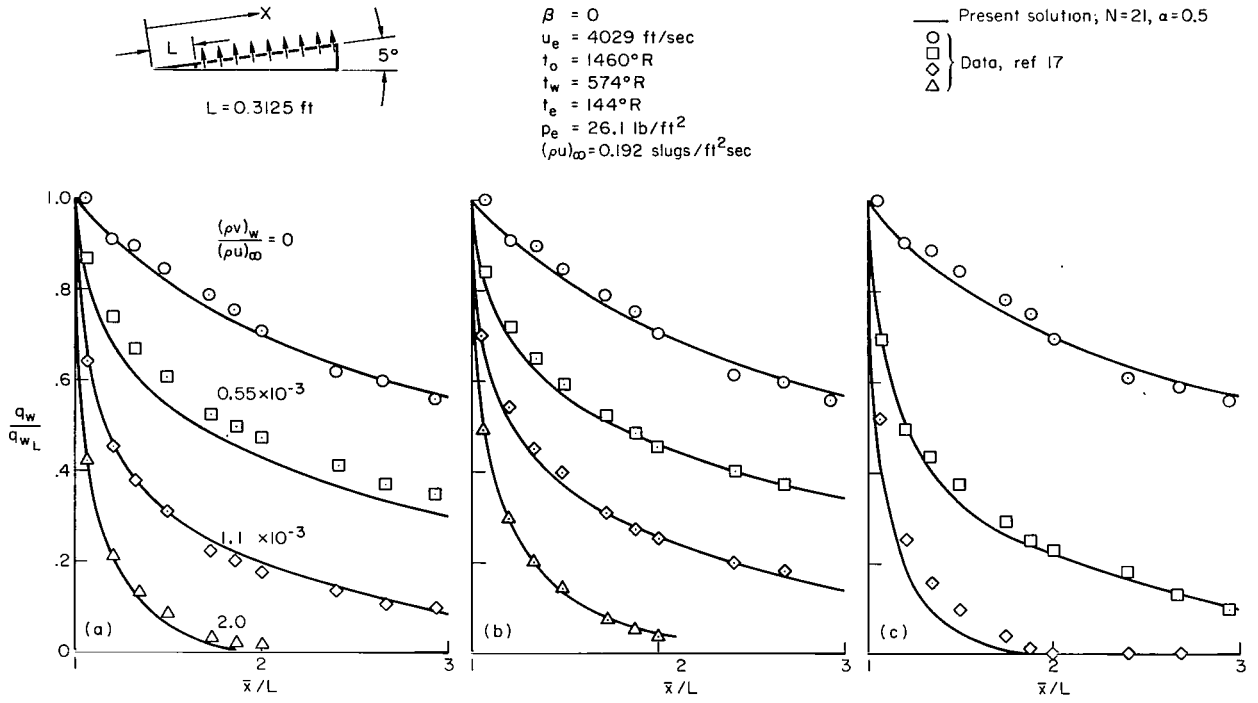

(a) Air injection.
(b) Argon injection.
(c) Helium injection.

Figure 5.- Comparison of present solution with heat-transfer data on a sharp 5° porous cone, reference 17.

CONCLUDING REMARKS

An accurate numerical method was developed for solving the nonsimilar boundary-layer equations, including binary gas injection. The conservation equations in the familiar Levy-Lees coordinates were transformed to new coordinates having a finite domain. By the appropriate choice of implicit finite difference expressions, the governing partial differential equations and boundary conditions were reduced to a set of linear algebraic equations in terms of the dependent variables only and a single stream function equation. Initial values of the dependent variables required to solve the nonsimilar equations were determined by applying the same method to solve the similarity form of the boundary-layer equations.

The capabilities and accuracy of the method were demonstrated by comparison with other numerical solutions and with experimental data. The comparisons showed that the present method could be accurately applied to a variety of examples. The method is ideally suited to solving flow problems where skin friction and heat transfer become small, as in the case of boundary-layer injection.

Additional information regarding the computer program details can be obtained by contacting the authors.

Ames Research Center
National Aeronautics and Space Administration
Moffett Field, Calif. 94035, July 16, 1969

APPENDIX A

FINITE DIFFERENCE AND MATRIX ELEMENT EQUATIONS

FOR THE NONSIMILAR BOUNDARY-LAYER EQUATIONS

The following finite-difference equations were used to reduce the nonsimilar boundary-layer equations to a system of linear algebraic equations. The appropriate grid system from sketch (b) is reproduced here with redundant grid notation for convenience in writing the difference equations.

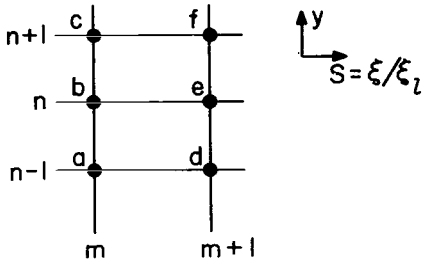

Sketch (b)

$$G = G_e \tag{A1}$$

$$G_S = \frac{G_e - G_b}{\Delta S} \tag{A2}$$

$$G_y = \frac{1}{4\ \Delta y}\left(G_c - G_a + G_f - G_d\right) \tag{A3}$$

$$G_{yy} = \frac{1}{2(\Delta y)^2}\left(G_c - 2G_b + G_a + G_f - 2G_e + G_d\right) \tag{A4}$$

$$R_y = \frac{R_c - R_a}{2\ \Delta y} \tag{A5}$$

$$R_{yy} = \frac{R_c - 2R_b + R_a}{(\Delta y)^2} \tag{A6}$$

$$GM_S = G_b\,\frac{(M_e - M_b)}{\Delta S} \tag{A7}$$

$$G_yM_y = \frac{1}{8(\Delta y)^2}\left[(G_c - G_a)(M_f - M_d) + (G_f - G_d)(M_c - M_a)\right] \tag{A8}$$

$$G_y{}^2 = \frac{1}{4(\Delta y)^2}\left[(G_c - G_a)(G_f - G_d)\right] \tag{A9}$$

$$G^2 = G_bG_e \tag{A10}$$

$$GM_y = G_b \left\{ \frac{1}{4\,\Delta y} \left[(M_c - M_a) + (M_f - M_d) \right] \right\} \tag{A11}$$

Equations (A2) through (A4), the Crank-Nicholson formulas, are used to approximate the unknowns and derivatives of the unknowns. The central difference equations, (A5) and (A6), are used to approximate derivatives of the properties. Equations (A7) through (A11) were chosen so that the unknowns appear linearly.

These difference equations are substituted into equations (9) through (11) to obtain

Momentum:

$$A_{11}F_d + B_{11}F_e + C_{11}F_f = D_1 \tag{A12}$$

Energy:

$$A_{22}T_d + B_{22}T_e + C_{22}T_f + A_{21}F_d + B_{21}F_e + C_{21}F_f + A_{23}C_{1_d} + C_{23}C_{1_f} = D_2 \tag{A13}$$

Species:

$$A_{33}C_{1_d} + B_{33}C_{1_e} + C_{33}C_{1_f} = D_3 \tag{A14}$$

Expressions for the coefficients are presented below. There are $3(N - 2)$ equations for N nodal points and these are conveniently expressed by the matrix equation

$$A_n\bar{\bar{\omega}}_{n-1} + B_n\bar{\bar{\omega}}_n + C_n\bar{\bar{\omega}}_{n+1} = \bar{\bar{D}}_n \qquad n = 2, 3, \ldots, N - 1 \tag{A15}$$

where

$$\bar{\bar{\omega}}_n = \begin{bmatrix} F_e \\ T \\ C_1 \end{bmatrix}_{n,m+1} \qquad \bar{\bar{D}}_n = \begin{bmatrix} D_1 \\ D_2 \\ D_3 \end{bmatrix}_{\substack{n,m \\ \text{or } n,m+1/2}}$$

$$A_n = \begin{bmatrix} A_{11} & 0 & 0 \\ A_{21} & A_{22} & A_{23} \\ 0 & 0 & A_{33} \end{bmatrix}_{\substack{n,m \\ \text{or } n,m+1/2}} \qquad B_n = \begin{bmatrix} B_{11} & 0 & 0 \\ B_{21} & B_{22} & 0 \\ 0 & 0 & B_{33} \end{bmatrix}_{\substack{n,m \\ \text{or } n,m+1/2}}$$

$$C_n = \begin{bmatrix} C_{11} & 0 & 0 \\ C_{21} & C_{22} & C_{23} \\ 0 & 0 & C_{33} \end{bmatrix}_{\substack{n,m \\ \text{or } n,m+1/2}}$$

The matrix elements are given in the following equations, where for convenience, Z replaces the term $\alpha(1 - y)$. Also it is to be noted that following the first iteration quantities not subscripted with b are evaluated at (n, m + 1/2) by averaging quantities at n, m with those at (n, m + 1).

$$A_{11} = \left[\frac{\phi Z^2}{2\,\Delta y^2} + \frac{Z}{4\,\Delta y}\left(-Z\phi_y + \alpha\phi - f - 2Sf_S\right)\right]$$

$$B_{11} = \left[-\frac{\phi Z^2}{(\Delta y)^2} + F_b\left(-\frac{2S}{\Delta S} - \beta\right)\right]$$

$$C_{11} = \left(-A_{11} + \frac{\phi Z^2}{\Delta y^2}\right)$$

$$D_1 = \left[-\frac{\phi Z^2}{2}(F_b)_{yy} + \frac{Z(Fb)_y}{2}\left(-Z\phi_y + \alpha\phi - f - 2Sf_S\right) - \frac{2SF_b{}^2}{\Delta S} - \beta\frac{\rho_e}{\rho}\right]$$

$$A_{22} = \left\{\frac{\phi Z^2}{2Pr\,\Delta y^2} + \frac{Z}{4\,\Delta y}\left[-\frac{Z}{C_p}\left(\frac{\phi C_p}{Pr}\right)_y + \frac{\phi\alpha}{Pr} - f - 2Sf_S - \frac{\phi Z\left(C_{p_1} - C_{p_2}\right)}{ScC_p}\left(C_{1_b}\right)_y\right]\right\}$$

$$B_{22} = \left(-\frac{\phi Z^2}{Pr\,\Delta y^2} - \frac{2SF_b}{\Delta S}\right)$$

$$C_{22} = \left(-A_{22} + \frac{\phi Z^2}{Pr\,\Delta y^2}\right)$$

$$A_{21} = \left[-\frac{\phi u_e{}^2 Z^2 (F_b)_y}{2C_p t_o\,\Delta y}\right]$$

$$B_{21} = \left(-\frac{\beta u_e{}^2}{C_p t_o}\frac{\rho_e}{\rho}\right)$$

$$C_{21} = -A_{21}$$

$$A_{23} = \left[-\frac{\phi\left(C_{p_1} - C_{p_2}\right)Z^2}{4\,\Delta y ScC_p}(T_b)_y\right]$$

$$C_{23} = (-A_{23})$$

$$D_2 = \left\{ - \frac{\phi Z^2}{2Pr} (T_b)_{yy} + \frac{Z}{2} (T_b)_y \left[- \frac{Z}{C_p} \left(\frac{\phi C_p}{Pr} \right)_y + \frac{\phi \alpha}{Pr} - f - 2Sf_S \right] - \frac{2SF_b T_b}{\Delta S} \right\}$$

$$A_{33} = \left\{ \frac{\phi Z^2}{2Sc\ \Delta y^2} + \frac{Z}{4\ \Delta y} \left[-Z \left(\frac{\phi}{Sc} \right)_y + \frac{\phi \alpha}{Sc} - f - 2Sf_S \right] \right\}$$

$$B_{33} = \left(- \frac{\phi Z^2}{Sc\ \Delta y^2} - \frac{2SF_b}{\Delta S} \right)$$

$$C_{33} = \left(-A_{33} + \frac{\phi Z^2}{Sc\ \Delta y^2} \right)$$

$$D_3 = \left\{ - \frac{\phi Z^2}{2Sc} \left(C_{1_b} \right)_{yy} + \frac{Z \left(C_{1_b} \right)_y}{2} \left[-Z \left(\frac{\phi}{Sc} \right)_y + \frac{\phi \alpha}{Sc} - f - 2Sf_S \right] - \frac{2SF_b{}^2 \left(C_1 \right)_b}{\Delta S} \right\}$$

APPENDIX B

FINITE DIFFERENCE AND MATRIX ELEMENT EQUATIONS

FOR THE SIMILAR BOUNDARY-LAYER EQUATIONS

The finite-difference equations used to reduce the similarity boundary-layer equations to a system of linear algebraic equations are given below. The grid system is shown in sketch (c) with redundant notation for convenience in writing the difference equations. The superscript (ν) is understood to be the iteration number.

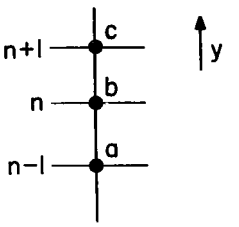

Sketch (c)

$$M_y = \frac{1}{2\,\Delta y}\,(M_c - M_a) \tag{B1}$$

$$M_{yy} = \frac{1}{(\Delta y)^2}\,(M_c - 2M_b + M_a) \tag{B2}$$

$$M^2 = M_b^{\nu+1} M_b^{\nu} \tag{B3}$$

$$G_y M_y = \frac{1}{8\,\Delta y^2}\left[(G_c - G_a)^{\nu+1}(M_c - M_a)^{\nu} + (M_c - M_a)^{\nu+1}(G_c - G_a)^{\nu}\right] \tag{B4}$$

$$(G_y)^2 = \frac{(G_c - G_a)^{\nu}(G_c - G_a)^{\nu+1}}{4\,\Delta y^2} \tag{B5}$$

Substituting the above difference equations into equations (9) through (11) with the right-hand sides set to zero and approximating $f(M)_y$ by $f_b^{\nu}(M)_y$ results in equations of the form given by equations (A12) to (A14). The expressions for matrix elements are

$$A_{11} = \left[-\frac{Z^2\phi_y^{\nu}}{2\,\Delta y} + \frac{Z^2\phi^{\nu}}{(\Delta y)^2} + \frac{\alpha Z\phi^{\nu}}{2\,\Delta y} - \frac{Zf_b^{\nu}}{2\,\Delta y}\right]$$

$$B_{11} = \left[- \frac{2Z^2 \phi^{\nu}}{(\Delta y)^2} - \beta F_b{}^{\nu} \right]$$

$$C_{11} = \left[-A_{11} + \frac{2Z^2 \phi^{\nu}}{(\Delta y)^2} \right]$$

$$D_1 = \left[-\beta \left(\frac{\rho_e}{\rho} \right) \right]$$

$$A_{22} = \left[- \frac{Z^2 \left(\frac{\phi C_p}{Pr} \right)_y^{\nu}}{C_p{}^{\nu} (2\ \Delta y)} + \frac{Z^2 \left(\frac{\phi}{Pr} \right)^{\nu}}{(\Delta y)^2} + \frac{\left(\frac{\phi}{Pr} \right)^{\nu} \alpha Z}{2(\Delta y)} - \frac{f_b{}^{\nu} Z}{2\ \Delta y} - \left(\frac{\phi}{ScC_p} \right)^{\nu} \frac{\left(C_{p_1} - C_{p_2} \right) \left(C_1 \right)_y^{\nu}}{4\ \Delta y} Z^2 \right]$$

$$B_{22} = \left[- \frac{2 \left(\frac{\phi}{Pr} \right)^{\nu} Z^2}{(\Delta y)^2} \right]$$

$$C_{22} = \left[-A_{22} + \frac{2Z^2}{(\Delta y)^2} \left(\frac{\phi}{Pr} \right)^{\nu} \right]$$

$$A_{21} = \left[- \frac{u_e{}^2 Z^2 \phi^{\nu}}{t_o C_p{}^{\nu}} \frac{(F)_y^{\nu}}{2(\Delta y)^2} \right]$$

$$B_{21} = \left(- \frac{u_e{}^2 \beta}{C_p{}^{\nu} t_o} \frac{\rho_e}{\rho} \right)$$

$$C_{21} = (-A_{21})$$

$$A_{23} = \left[-Z^2 \left(\frac{\phi}{ScC_p} \right)^{\nu} \frac{\left(C_{p_1} - C_{p_2} \right) (T)_y^{\nu}}{4\ \Delta y} \right]$$

$$C_{23} = (-A_{23})$$

$$D_2 = 0$$

$$A_{33} = \left[- \frac{Z^2\left(\frac{\phi}{Sc}\right)^{\nu}_{y}}{2\ \Delta y} + \frac{Z^2\left(\frac{\phi}{Sc}\right)^{\nu}}{\Delta y^2} + \frac{\alpha Z\left(\frac{\phi}{Sc}\right)^{\nu}}{2\ \Delta y} - \frac{f_b{}^{\nu} Z}{2\ \Delta y} \right]$$

$$B_{33} = \left[- \frac{2Z^2\left(\frac{\phi}{Sc}\right)^{\nu}}{(\Delta y)^2} \right]$$

$$C_{33} = \left[-A_{33} + \frac{2Z^2}{(\Delta y)^2} \left(\frac{\phi}{Sc}\right)^{\nu} \right]$$

$$D_3 = 0$$

REFERENCES

1. Clutter, Darwin W.; and Smith, A. M. O.: Solution of the General Boundary Layer Equations for Compressible Laminar Flow, Including Transverse Curvature. Douglas Aircraft Co. Rep. L.B. 31088, Feb. 15, 1963.

2. Jaffe, Nicholas A.; Lind, Richard C.; and Smith, A. M. O.: Solution to the Binary Diffusion Laminar Boundary-Layer Equations with Second-Order Transverse Curvature. AIAA J., vol. 5, no. 9, Sept. 1967, pp. 1563-1569.

3. Marvin, Joseph G.; and Sinclair, A. Richard: Convective Heating in Regions of Large Favorable Pressure Gradient. AIAA J., vol. 5, no. 11, Nov. 1967, pp. 1940-1948.

4. Gallo, William F.; Marvin, Joseph G.; and Gnos, A. Vernon: A Study of the Nonsimilar Nature of the Laminar Boundary Layer in a Region of Adverse Pressure Gradient. AIAA paper 69-35.

5. Moran, James P.; and Scott, Paul B.: A Mass Transfer Finite Difference Formulation Employing Crocco Variables. M.I.T. Tech. Rep. 443, June 1960.

6. Flügge-Lotz, I.; and Blottner, F. G.: Computation of the Compressible Laminar Boundary-Layer Flow Including Displacement Thickness Interaction Using Finite-Difference Methods. Stanford University Tech. Rep. 131, Jan. 1962.

7. Blottner, F. G.: Nonequilibrium Laminar Boundary Layer Flow of a Binary Gas. General Electric Co., Phila., Pa., Space Science Lab. R63SD17, June 1963.

8. Levine, J. N.: Finite Difference Solution of the Laminar Boundary Layer Equations Including Second-Order Effects. AIAA paper 68-739.

9. Moore, J. A.; and Lee, J. T.: Discontinuous Injection of Inert Gases Into the Nonequilibrium Laminar Boundary Layer. T.R.W. Rep. 06388-6018R000, July 1967. (In: International Astronautical Federation, International Astronautical Congress, 18th Belgrade, Sept. 24-30, 1967 Proceedings. Vol. 3 Propulsion and Re-entry, Oxford, Pergamon Press, 1968, pp. 247-269.)

10. Sills, J. A.: Transformations for Infinite Regions and Their Application to Flow Problems. AIAA J., vol. 7, no. 1, 1969.

11. Dorrance, William H.: Viscous Hypersonic Flow; Theory of Reacting and Hypersonic Boundary Layers. Ch. 10, McGraw-Hill Book Co., Inc., copyright 1962, pp. 277-279.

12. Varga, Richard S.: Matrix Iterative Analysis. Prentice Hall, Inc., Englewood Cliffs, N. J., 1962, pp. 194-197.

13. Hayasi, Nisiki: Displacement Thickness of the Boundary Layer with Blowing. AIAA J., vol. 3, no. 12, Dec. 1965, pp. 2348-2349.

14. Low, George M.: The compressible Laminar Boundary Layer With Fluid Injection. NACA TN 3404, 1955.

15. Baron, Judson R.: The Binary-Mixture Boundary Layer Associated with Mass Transfer Cooling at High Speeds. M.I.T. Tech. Rep. 160, May 1956.

16. Kendall, Robert M.; and Bartlett, Eugene P.: Nonsimilar Solution of the Multicomponent Laminar Boundary Layer by an Integral Matrix Method. AIAA paper 67-218.

17. Marvin, Joseph G.; and Akin, Clifford M.: Combined Effects of Mass-Addition and Nose-Bluntness on Boundary Layer Transition. AIAA paper 69-706.

NATIONAL AERONAUTICS AND SPACE ADMINISTRATION
WASHINGTON, D.C. 20546

OFFICIAL BUSINESS

FIRST CLASS MAIL

POSTAGE AND FEES PAID
NATIONAL AERONAUTICS AND
SPACE ADMINISTRATION

POSTMASTER: If Undeliverable (Section 158 Postal Manual) Do Not Return

"The aeronautical and space activities of the United States shall be conducted so as to contribute . . . to the expansion of human knowledge of phenomena in the atmosphere and space. The Administration shall provide for the widest practicable and appropriate dissemination of information concerning its activities and the results thereof."

—NATIONAL AERONAUTICS AND SPACE ACT OF 1958

NASA SCIENTIFIC AND TECHNICAL PUBLICATIONS

TECHNICAL REPORTS: Scientific and technical information considered important, complete, and a lasting contribution to existing knowledge.

TECHNICAL NOTES: Information less broad in scope but nevertheless of importance as a contribution to existing knowledge.

TECHNICAL MEMORANDUMS: Information receiving limited distribution because of preliminary data, security classification, or other reasons.

CONTRACTOR REPORTS: Scientific and technical information generated under a NASA contract or grant and considered an important contribution to existing knowledge.

TECHNICAL TRANSLATIONS: Information published in a foreign language considered to merit NASA distribution in English.

SPECIAL PUBLICATIONS: Information derived from or of value to NASA activities. Publications include conference proceedings, monographs, data compilations, handbooks, sourcebooks, and special bibliographies.

TECHNOLOGY UTILIZATION PUBLICATIONS: Information on technology used by NASA that may be of particular interest in commercial and other non-aerospace applications. Publications include Tech Briefs, Technology Utilization Reports and Notes, and Technology Surveys.

Details on the availability of these publications may be obtained from:

SCIENTIFIC AND TECHNICAL INFORMATION DIVISION

NATIONAL AERONAUTICS AND SPACE ADMINISTRATION

Washington, D.C. 20546